Femtosecond pulse propagation in air: Variational analysis

N. Aközbek and C. M. Bowden
U.S Army Aviation and Missile Command, Weapons Sciences Directorate, Missile Research Development and Engineering Center, Redstone Arsenal, Huntsville, Alabama 35898-5000

A. Talebpour and S. L. Chin
Centre d'Optique, Photonique et Laser and Département de Physique, Université Laval, Quebec City, Quebec, Canada G1K 7P4
(Received 14 September 1999; revised manuscript received 22 November 1999)

We use a variational method to study the phenomenon of intense femtosecond pulse propagation in air. This method allows us to obtain a semianalytical solution to the problem in which a wide range of initial conditions can be studied. In addition, it provides a simple physical interpertation, where the problem is reduced to an analogous problem of a particle moving in a potential well. Different types of possible solutions are considered, with focus upon the main physical interpretations. The results recapture at least qualitatively some of the major experimental observations, and previous numerical simulations.

PACS number(s): 42.65.Jx, 52.35.Mw

I. INTRODUCTION

In the last several years, there has been an interest in the propagation of femtosecond pulses in air undergoing multiphoton ionization [1–8]. Experimental studies in the laboratory have shown that such pulses can propagate tens of meters [1–3], beyond the Rayleigh range of the laser beam. In fact it has been suggested that these pulses propagate up to 12 km in the atmosphere, based upon experimental studies by the group in Jena, Germany [4]. The detailed characteristic of the produced filament is not known in their experiment, but they do observe the generation of white-light along the filament. Applications of this phenomenon include remote sensing [4] and lightning discharge control [8].

The problem is complicated in general since it involves pulses that are on the order of the femtosecond scale and undergo strong spatial and temporal reshaping. In addition, the field interacts strongly with the medium, leading to multiphoton ionization of air molecules, which in turn creates a plasma. This is a regime not widely studied, in which both the temporal as well as spatial dynamics of the laser are equally important and cannot be separated from each other.

It has been suggested that the underlying physical mechanism leading to the long-range propagation is a dynamic balance between self focusing and defocusing, created by the plasma via multiphoton ionization. Several models in this respect including the self-guided pulse propagation [1,2], modified moving-focus model [3] and dynamic spatial replenishment [5] have been proposed. Due to the fact that the dynamics is complicated it has not been easy to interpret the experimental results through numerical simulations using the nonlinear Schrödiger equation.

Our aim here is to make a qualitative analytical assessment of the problem and to provide direct physical insight to an otherwise complicated problem. Particularly, our aim is to show that the defocusing created by the plasma generation behaves like an effective higher-order nonlinear susceptibility, $\chi^{(n)}$. This explicit connection will provide a better understanding on how the balance between self focusing and defocusing is created and its consequence on the pulse propagation. Our methods are based on the variational method, which has been successfully implemented in various propagation problems such as self focusing in a bulk medium [9], and pulse propagation in dissipative systems [10]. It has the advantage of providing a semi-analytical result without resorting to lengthy computational simulations.

Since the plasma generation plays an important role in the defocusing mechanism it is important that the multiphoton ionization model based on direct experimental measurements for the constituents of air, namely nitrogen and oxygen be used in numerical simulations. In previous numerical simulations, multiphoton ionization models based on Szöke, ADK (Ammasov, Delone, Kraniov) and Keldysh models have been used to describe the multiphoton ionization in air. Using these models some of the experimental results can be explained qualitatively, however for more realistic calculations it is necessary to use an ionization model that agrees well with the experiment. A semiempirical model has been obtained for the ionization rates of nitrogen and oxygen [11], which we will make use of in our calculations.

We will show using our analytical model how the self focusing and defocusing created by the generated plasma via multiphoton ionization can lead to a long distance propagation. Our analysis is not restricted to pulse propagation in an ionizing medium but can also be applied to pulse propagation in a medium that exhibits higher-order defocusing effects arising from a different physical origin. This makes our approach more general in that certain results can be connected to other studies related to laser beam propagation in a medium that exhibits higher-order defocusing effects. Despite the simplicity and approximations employed in our calculations, the results are at least qualitatively in good agreement with experimental observations and previous numerical simulations.

II. MODEL

Here, we consider the propagation of a linearly polarized laser beam in air. From Maxwell's equations we obtain the following scalar wave equation [12]

$$\frac{\partial^2 E}{\partial z^2}+\frac{\partial^2 E}{\partial x^2}+\frac{\partial^2 E}{\partial y^2}-\frac{\epsilon_0}{c^2}\frac{\partial^2 E}{\partial t^2}-\frac{4\pi}{c^2}\frac{\partial^2 P_{NL}}{\partial t^2}-\frac{4\pi}{c^2}\frac{\partial J}{\partial t}=0. \tag{1}$$

Here, $P_{NL}=\chi^{(3)}E^3+\chi^{(5)}E^5$ is the nonlinear polarization, where $\chi^{(3)}$ and $\chi^{(5)}$, respectively, are the third and fifth order nonlinear susceptibility coefficients of the medium, and ϵ_0 is the linear dielectric constant of air. The strong interaction of the radiation field with the air molecules produces an electron density, through the multiphoton ionization process, that in the Drude model can be described by the current density as $J=\sigma E$, where $\sigma=\sigma_0/(1-i\omega\tau_{col})$ is the conductivity and $\sigma_0=N_e e^2\tau_{col}/m_e$ [12]. Here, N_e is the electron density and τ_{col} is the collision time of the electrons in air, which is on the order of picoseconds. The electric field can be written as

$$E(x,y,z,t)=\mathcal{E}(x,y,z,t)e^{ikx-i\omega t}+\text{c.c.}, \tag{2}$$

where $\mathcal{E}$ is assumed to be a slowly varying envelope function. Using Eq. (2) in Eq. (1) and applying the slowly varying envelope approximation, Eq. (1) takes the following form in the retarded coordinate system ($\tau=t-z/v_g$ and $v_g=c/\sqrt{\epsilon_0}$):

$$i\frac{\partial\mathcal{E}}{\partial z}+\frac{1}{2k}\left(\frac{\partial^2\mathcal{E}}{\partial x^2}+\frac{\partial^2\mathcal{E}}{\partial y^2}\right)+\Delta n\mathcal{E}+i\left[\frac{2\pi e^2 N_e(|\mathcal{E}|^2)}{km_e c^2\omega\tau_{col}}+\Gamma_{\text{MPA}}|\mathcal{E}|^{2n-2}\right]\mathcal{E}=0 \tag{3}$$

and

$$\Delta n=n_2 k_0|\mathcal{E}|^2-n_4 k_0|\mathcal{E}|^4-\frac{2\pi e^2 N_e(|\mathcal{E}|^2)}{km_e c^2}. \tag{4}$$

Here, $n_2=12\pi^2\chi^{(3)}/n_0^2 c$, and $n_4=80\pi^3|\chi^{(5)}|/n_0^3 c^2$, which are given in units of cm^2/W and cm^4/W^2, respectively, and $n_0=\sqrt{\epsilon_0}$ is the index of refraction of air. The last term in Δn comes from the contribution of the plasma, where we assumed that $\omega\tau_{col}\gg 1$. The last two terms in Eq. (3) represent absorption by the plasma and multiphoton absorption losses, respectively, where $\Gamma_{\text{MPA}}=N_0\sigma^{(n)}/2n\hbar\omega$. The generated electron density, N_e is governed by

$$\frac{\partial N_e}{\partial\tau}=N_0 R(|\mathcal{E}|^2). \tag{5}$$

Here N_0 is the density of neutral atoms, and $R(|\mathcal{E}|^2)=\sigma^{(n)}|\mathcal{E}|^{2n}$ is the rate of ionization for nitrogen (oxygen), where n is the effective order of the ionization process, which is determined from direct experimental measurements [11]. We assume that air is a mixture of nitrogen (80%) and oxygen (20%). Equation (5) can be integrated to yield

$$N_e=\int_{-\infty}^{\tau}N_0\sigma^{(n)}|\mathcal{E}|^{2n}d\tau'. \tag{6}$$

Using a simple integration rule, the electron density can be approximated for an integration up to the peak of the pulse, as $N_e=g(\tau)N_0\sigma^{(n)}|\mathcal{E}|^{2n}$, where $g(\tau)=0.5(\tau_{\min}+\tau)$. Here, $\tau_{\min}$ is a cutoff determined by the initial pulse. It is important to note that the electron density has to be evaluated at each propagation distance, which does not pertain in this case. However, as we will demonstrate later most of the important physics is still retained in this approximation. Making this approximation not only simplifies the calculations but also makes the interpretation more transparent. Then Eq. (3) can be written as

$$i\frac{\partial\mathcal{E}}{\partial z}+\frac{1}{2k}\left(\frac{\partial^2\mathcal{E}}{\partial x^2}+\frac{\partial^2\mathcal{E}}{\partial y^2}\right)+\alpha|\mathcal{E}|^2\mathcal{E}-\beta|\mathcal{E}|^4\mathcal{E}-\gamma|\mathcal{E}|^{2n}\mathcal{E}+i(\Gamma_{\text{P}}|\mathcal{E}|^{2n}+\Gamma_{\text{MPA}}|\mathcal{E}|^{2n-2})\mathcal{E}=0, \tag{7}$$

where $\alpha=n_2 k_0$, $\beta=n_4 k_0$, $\gamma=2\pi e^2/km_e c^2 N_0\sigma^{(n)}g(\tau)$, and $\Gamma_{\text{P}}=2\pi e^2 g(\tau)N_0\sigma^{(n)}/km_e c^2\omega\tau_{col}$. Equation (7) describes the propagation of an intense femtosecond pulse in the presence of a self-induced plasma and possible higher-order nonresonant nonlinear effects $\chi^{(5)}$, arising from the higher-order polarizability of the air molecules. Equation (7) includes the most important physical ingredients of the more general propagation problem, such as diffraction, self focusing and defocusing. Here, we use parameters close to the experiment performed at Laval University [7] in order to make a qualitative comparison with their results. We consider the propagation of a 800 nm laser pulse with a pulse duration of 220 fs [full width at half maximum (FWHM)]. The nonlinear index of refraction for air is taken as $n_2=4.0\times10^{-19}$ cm^2/W [13] corresponding to a critical power $P_{cr}=2.5$ GW, where $P_{cr}=\lambda_0^2/2\pi n_0 n_2$ is the critical power for self focusing for a CW beam in a simple Kerr medium. The density of neutral atoms in air is taken to be $N_0=3.0\times10^{19}$ cm^{-3}. The multiphoton ionization transition rates were obtained from the experiments at Laval University. We find that their experimental data can be fitted to the form $\sigma^{(n)}|\mathcal{E}|^{2n}$, that is valid in the intensity range of 10^{13} W/cm^2 to 2.0×10^{14} W/cm^2. This yields for oxygen $\sigma^{(n)}=1.29\times10^{-65}$ $\text{s}^{-1}(\text{cm}^2/\text{W})^n$ with $n=5.51$ and for nitrogen $\sigma^{(n)}=4.45\times10^{-84}$ s^{-1} $(\text{cm}^2/\text{W})^n$ with $n=6.78$ [11]. Since there is no experimental data available below 10^{13} W/cm^2, we do not know if the slopes can be extended to lower intensities. However, in our analysis it is estimated that self focusing is mostly dominant up to 10^{13} W/cm^2. Thus the plasma contribution may be neglected below 10^{13} W/cm^2. From the fitted slopes, it turns out that oxygen is more dominant in the plasma generation than nitrogen, which is reasonable in view of the lower ionization potential of O_2 (12.1 eV) as compared to that of N_2 (15.58 eV). In our model we have included the next higher-order nonlinear term of the susceptibility function, corresponding to a $\chi^{(5)}$ effect. Information on the sign and magnitude on higher-order nonlinear susceptibilities are not as widely available as $\chi^{(3)}$. However, in this paper we will use an estimated value for $\chi^{(5)}$ and determine its effect on the pulse propagation. One possible estimate for $\chi^{(5)}$ can be estimated from the fact that $\chi^{(5)}\sim 1/E_{at}^4$ and $\chi^{(3)}\sim 1/E_{at}^2$ where $E_{at}\simeq 10^6$ statvolt/cm is the atomic electric field strength, then $\chi^{(5)}/\chi^{(3)}\sim 10^{-12}$ [14] (for nonresonant interactions). For typical gases $\chi^{(3)}\sim 10^{-18}-10^{-17}$(esu) then $\chi^{(5)}\sim 10^{-30}-10^{-29}$(esu). This is only an estimate for the mag-

nitude of $\chi^{(5)}$ but does not give any information on the sign. Some numerical and experimental studies have been done for some gases in regard to higher-order harmonic generation. For some noble gases such as Ar, $|\chi^{(5)}| \simeq 10^{-29}$(esu) and Xe, $|\chi^{(5)}| \simeq 10^{-28}$(esu) ($\lambda_0 = 1064$ nm, 694 nm) [15,16], whose ionization energies are close to nitrogen and oxygen, respectively. In our calculations we will use $|\chi^{(5)}| \simeq -3.6 \times 10^{-29}$(esu) which corresponds to $n_4 = 10^{-32}$ cm^4/W^2 and determine qualitatively its contribution to the defocusing in addition to the plasma generation via multiphoton ionization. It is important to note that the magnitude and sign of $\chi^{(5)}$ strongly depends on the laser frequency as well as on the structure of the atomic spectrum.

A. Variational method

Equation (3) in general must be solved together with Eq. (5) numerically. However, in regard to Eq. (7) the problem can be solved by using a variational method. The variational approach is only an approximation and is as good as the initial trial solution. However, the advantage of this approach is that it provides a semianalytical result that can be analyzed much easier and in most cases gives a simple physical insight to the problem. The variational method is based on defining a Lagrangian functional for the system from which the equations of motions can be derived.

Let us write the total Lagrangian as

$$\mathcal{L} = \mathcal{L}_C + \mathcal{L}_{NC}, \tag{8}$$

where $\mathcal{L}_C$ denotes the conservative and $\mathcal{L}_{NC}$ the nonconservative part of the total Lagrangian, respectively. Equation (7) can be derived from the Lagrangian in the presence of losses as [10]:

$$\frac{\delta \mathcal{L}}{\delta \mathcal{E}^*} = \frac{\partial}{\partial z}\left[\frac{\partial \mathcal{L}_C}{\partial\left(\frac{\partial \mathcal{E}^*}{\partial z}\right)}\right] - \frac{\partial \mathcal{L}_C}{\partial \mathcal{E}^*} = Q, \tag{9}$$

where

$$\mathcal{L}_C = \frac{i}{2}\left(\mathcal{E}\frac{\partial \mathcal{E}^*}{\partial z} - \mathcal{E}^*\frac{\partial \mathcal{E}}{\partial z}\right) + \frac{1}{2k}\left(\left|\frac{\partial \mathcal{E}}{\partial x}\right|^2 + \left|\frac{\partial \mathcal{E}}{\partial y}\right|^2\right) - \frac{\alpha}{2}|\mathcal{E}|^4 + \frac{\beta}{3}|\mathcal{E}|^6 + \frac{\gamma}{(n+1)}|\mathcal{E}|^{2n+2} \tag{10}$$

and $Q = -i\Gamma_{\mathrm{MPA}}|\mathcal{E}|^{2n-2}\mathcal{E} - i\Gamma_{\mathrm{P}}|\mathcal{E}|^{2n}\mathcal{E}$. In general, $\mathcal{E}$ can be expanded in terms of a complete set of eigenfunctions. However, here we restrict ourselves to the following trial solution for the electric field envelope,

$$\mathcal{E}(z,x,y,\tau) = A(z,\tau)e^{-(x^2+y^2)/a^2(z,\tau)}e^{ib(z,\tau)(x^2+y^2)+i\phi(z,\tau)}. \tag{11}$$

Here, A, a, b, and ϕ are variational parameters and depend both on z and τ. These variational parameters are sufficient to describe the dynamics of the problem, including the effect of self-phase modulation through $b(z,\tau)$. We consider a collimated input laser pulse focused by a lens. The focused field is assumed to be

$$\mathcal{E}(0,x,y,\tau) = \mathcal{E}_0 e^{-\tau^2/\tau_0^2 + (x^2+y^2)/a_0^2 - ik(x^2+y^2)/2f}. \tag{12}$$

Here, the pulse length at full width at half maximum (FWHM) of the irradiance is given by $\tau_{FWHM} = \sqrt{2\ln 2}\,\tau_0$, (for $\tau_{FWHM} = 220$ fs, $\tau_0 = 187$ fs), a_0 is defined as the beam radius at $1/e^2$ of the irradiance, and f is the focal length of the lens. The Rayleigh range (diffraction length) of the input beam is defined as $z_R = ka_0^2/2 = \pi a_0^2 n_0/\lambda_0 \simeq 4 \times 10^4 a_0^2$ for $\lambda_0 = 800$ nm.

In what follows, we neglect the absorption losses due to the plasma ($\Gamma_{\mathrm{P}} = 0$). In general this may not be the case and losses due to the plasma should be included in more quantitative numerical calculations. Inserting the trail solution (11) into the Lagrangian (10) and integrating over the transverse coordinate we obtain the reduced Lagrangian $\langle \mathcal{L}_C \rangle(z,\tau) = \int \mathcal{L}_C dx\, dy$, which depends only on the variational parameters and the independent variables z and τ. The equations of motion for those variational parameters in the presence of MPA, are found from [10],

$$\frac{\partial}{\partial \mu_i}\left(\frac{\partial \langle \mathcal{L}_C \rangle}{\partial \mu_{iz}}\right) - \frac{\partial \langle \mathcal{L}_C \rangle}{\partial \mu_i} = 2\,\mathrm{Re}\int Q\frac{\partial \mathcal{E}^*}{\partial \mu_i}dx\,dy, i = 1, \ldots, 4, \tag{13}$$

where $\mu_i = A, a, b, \phi$ $(i = 1, \ldots, 4)$. This leads to the following set of coupled equations:

$$\frac{\partial a}{\partial z} = 2ba + \Gamma_{\mathrm{MPA}} k \frac{2^n P_{cr}^{n-1}}{n\pi^{n-1}a_0^{2n-4}}\frac{P^{n-1}}{a^{2n-3}}\left(1 - \frac{a_0^4}{2n}\right) \tag{14}$$

$$\frac{\partial P}{\partial z} = -\Gamma_{\mathrm{MPA}} k \frac{2^n P_{cr}^{n-1}}{n\pi^{n-1}a_0^{2n-4}}\frac{P^n}{a^{2n-2}} \tag{15}$$

$$\frac{\partial b}{\partial z} = \frac{2}{a^4} - 2b^2 - \frac{2P}{a^4} + \left[\frac{4\gamma n k 2^n P_{cr}^n}{\pi^n (n+1)(2n+2)a_0^{2n-2}}\right]\frac{P^n}{a^{2n+2}} + \left(\frac{16\beta k P_{cr}^2}{9\pi^2 a_0^2}\right)\frac{P^2}{a^6}. \tag{16}$$

Equations (14)–(16) are rescaled so that they are in dimensionless units: z is in units of ka_0^2, $a/a_0 \to a$, $ba_0^2 \to b$, $\tau/\tau_0 \to \tau$, and $P/P_{cr} \to P$. Here, the total power $P = \int |\mathcal{E}|^2 dxdy = A^2 a^2 \pi/2$, and $P_{cr} = \lambda_0^2/2\pi n_0 n_2$ is the critical power for self focusing for a CW laser beam. Consider first the case of no losses ($\Gamma_{\mathrm{MPA}} = 0$) then from Eq. (15) it can be seen that the total power is conserved along the direction of propagation, so that $P(z,\tau) = P_0(\tau)$. In this case Eqs. (14)–(16) can be combined to give

$$\frac{1}{2}\left(\frac{\partial a}{\partial z}\right)^2 + U(a) = 0, \tag{17}$$

where

$$U(a)=\frac{2}{a^2}-\frac{2P_0(\tau)}{a^2}+\left[\frac{8\gamma nkP_{cr}^n 2^n}{2n\pi^n(n+1)(2n+2)a_0^{2n-2}}\right]\frac{P_0^n(\tau)}{a^{2n}}+\left(\frac{8\beta kP_{cr}^2}{9\pi^2 a_0^2}\right)\frac{P_0^2(\tau)}{a^4}+C(\tau) \tag{18}$$

and $C(\tau)$ is a constant of integration determined by the initial conditions

$$C(\tau)=-2+2P_0(\tau)-\left[\frac{8\gamma nk2^nP_{cr}^n}{2n\pi^n(n+1)(2n+2)a_0^{2n-2}}\right]P_0^n(\tau)-\left(\frac{8\beta kP_{cr}^2}{9\pi^2 a_0^2}\right)P_0^2(\tau)-2b_0^2. \tag{19}$$

Here, b_0 describes the initial wave front divergences of the laser beam, i.e., for a collimated beam $b_0=0$. Equation (17) describes the motion of a classical particle moving in a potential well $U(a)$.

Here, a describes the position of the particle, and z acts as a fictitious time variable. As we can see from Eq. (18) in the absence of defocusing effects the initial beam radius as well as critical power does not appear explicitly in the equations, however, in the presence of defocusing effects the equations are dependent on the initial beam radius as well as critical power. This dependence scales in powers of n, in other words small changes in these parameters could result in significantly different results.

B. Self-focusing in a simple Kerr Medium ($\gamma=\beta=0$)

Neglecting ionization and higher-order nonlinearity ($\gamma=\beta=0$), Eq. (17) can be integrated exactly to yield (here we assume an initially collimated beam so that $b_0=0$)

$$a(z,\tau)=\sqrt{1-4(P_0(\tau)-1)z^2} \tag{20}$$

The intensity is then easily found as

$$I(z,\tau)=\frac{2P_0}{\pi a^2}=\left(\frac{2}{\pi}\right)\frac{P_0(\tau)}{1-4[P_0(\tau)-1]z^2}. \tag{21}$$

Considering the CW case ($\tau=0$) it can easily be seen from Eq. (20) that when the initial power $P_0<1$, the beam radius $a(z)$ increases with z (diffraction), whereas when $P_0>1$ the beam radius decreases with z (self focusing) and collapses $[a(z_c)=0]$ at a finite distance given by $z_c=0.5/\sqrt{P_0-1}$ (in units of ka_0^2).

When the input power is time dependent it is known that self focusing leads to the compression of the pulse [17]. This effect can be seen in Fig. 1, where the on-axis temporal intensity profile is plotted as a function of the propagation distance. Clearly, as the pulse approaches the distance of collapse, it has been significantly compressed due to self focusing.

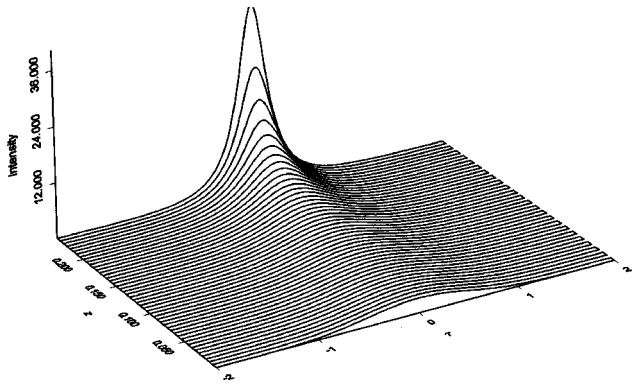

FIG. 1. Plotted is the on-axis temporal intensity (in units of P_{cr}/a_0^2) profile in the retarded coordinate τ (in units of τ_0) as a function of propagation distance z (in units of ka_0^2) for the case of a pulsed laser beam propagating in a simple Kerr medium. Pulse compression due to self-focusing can clearly be seen when the self-focal point is approached.

C. Self-focusing in a Kerr medium in the presence of self-induced plasma ($\beta=0,\gamma\neq 0$)

As the intensity increases during the self-focusing process, at high-enough intensities higher-order effects such as negative $\chi^{(5)}$ or the generation of a plasma will become important in stopping the selffocusing by defocusing the beam. It is clear from the experimental observations that the plasma generation plays an important role in the defocusing process. Although the plasma generation is only approximately incorporated into our model the results are in agreement with experimental observations. We neglect the contribution from $\chi^{(5)}$ ($\beta=0$), but will come back to this effect later. Below we discuss in detail the effect of the plasma generation on the beam dynamics by first considering the dynamics of one temporal slice ($\tau=0$), and then analyzing both the temporal and spatial dynamics of the laser pulse.

1. Dynamics of one time slice ($\tau=0$) of the pulse

First we consider the dynamics of the central part of the pulse, $P_0(0)=P_0$, then $g(0)=1$ where we have taken $\tau_{\min}=2$, and consider a collimated input laser beam ($b_0=0$). Depending on the initial condition there are several possible solutions. Keeping the input power $P_0=10$ (in units of P_{cr}) fixed we vary the initial beam radius a_0. As can be seen in Eq. (18) the effect of the defocusing depends on the initial beam radius. In Fig. 2(a), we plot the potential $U(a)$ as a function of the beam radius a (in units of a_0) for an initial beam radius $a_0=0.05$ cm. The solution corresponds to the case in which the particle is released from rest at the position $a=1$. If there is no defocusing effect it can be seen that the potential diverges [see Fig. 2(a) (dotted-line)], which causes catastrophic beam collapse. However, in the presence of defocusing around $a\simeq 0.55$ the defocusing starts to overcome the self focusing and eventually stops the selffocusing where the particle comes to rest at $a_{\min}$, where $U(a_{\min})=0$. Since there are no losses considered, the total energy is conserved, and the particle will come back to its initial position ($a=1$). This will continue in a periodic manner. In Fig. 2(b) the position of the particle $a(z)$ (beam radius), which is

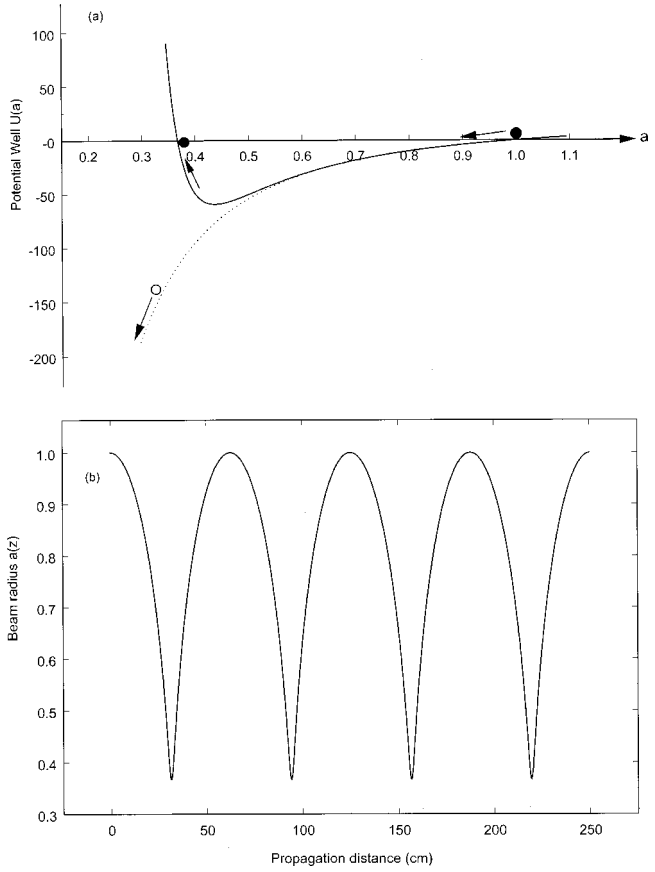

FIG. 2. Shown are (a) the potential $U(a)$ in which the particle moves as a function of a, and (b) the beam radius $a(z)$ (in units of the initial beam radius a_0) as a function of propagation distance z. The initial beam radius is $a_0=0.05$ cm and $P_0=10$. The solution corresponds to the case where the particle is released from $a=1$ at rest. When there is no defocusing effect the potential diverges (dotted line) and the particle (open circle) rolls towards $a=0$, i.e., the beam radius approaches zero (beam collapse). However, in the presence of defocusing there is significant change in which the defocusing effect becomes dominant at some position and stops the focusing at a_{min} (solid line). Here the particle (solid circle) will oscillate between $a=1$ and a_{min}. If there are no losses these oscillations will continue indefinitely. This oscillation manifests itself as a focusing and defocusing of the beam radius shown in (b).

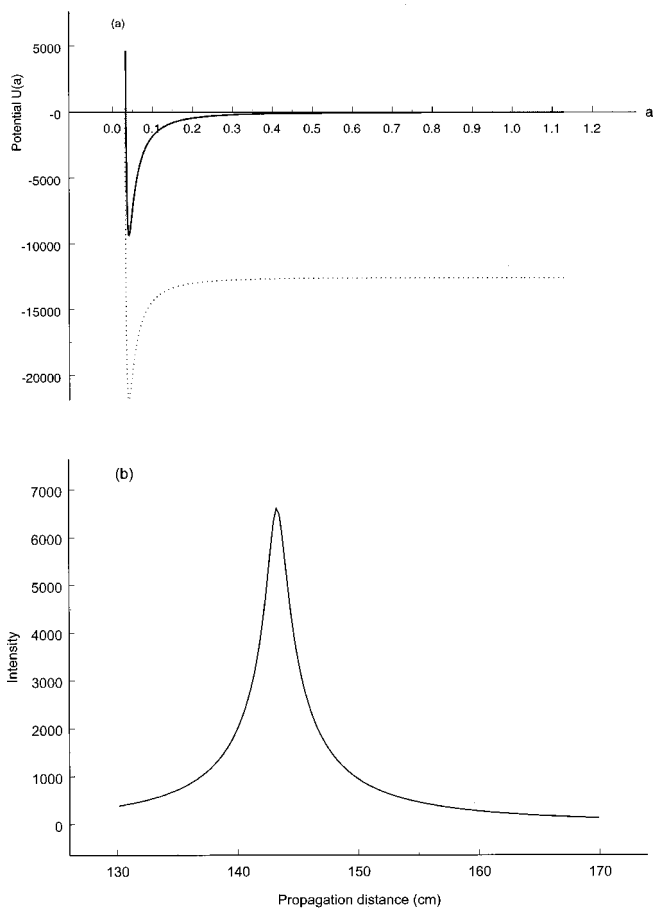

FIG. 3. Plotted is (a) the potential $U(a)$ for a laser beam with $a_0=0.55$ cm and $P_0=10$ and (b) the peak intensity (in units of P_{cr}/a_0^2) as a function of the propagation distance. In the case of an initially collimated beam the potential crosses the axis at two points (a) (solid line), whereas for an initially converging beam (focus by a converging lens with $f=150$ cm) the potential crosses the axis at one point only (a) (dotted line). For the case of an initially converging beam the solution corresponds to case where the particle is initially pushed (dotted line) and comes to rest at some a_{min}. However, since the potential does not cross the axis again the particle escapes to infinity and the beam diffracts. The solution to this case is given in (b) where the peak intensity is plotted as function of distance. As it can be seen the particle focuses once and then rapidly defocuses, in agreement with the potential analogy.

found by solving Eq. (17) numerically, is plotted as function of propagation distance z, in agreement with the potential analogy.

As the initial beam radius is decreased to some $a_0=a_s$ (for fixed P_0) the minimum point of the potential in Fig. 2(a) will move and coincide exactly at $a=1$, where $U(a)=0$. In this case the beam diameter remains unchanged during propagation. This condition can be found from $dU/da|_{a=1}=0$, which leads to the following relation between the power and beam radius:

$$\left[\frac{8\gamma n^2 k P_{cr}^n 2^n}{2n\pi^n(n+1)(2n+2)a_s^{2n-2}}\right]P_s^n-2P_s+2=0. \quad (22)$$

Here, P_s is the power of the self-trapped beam with a beam radius of a_s. When $\gamma=0$ the condition reduces to the one for a simple Kerr medium, $P_s=1$ (in units P_{cr}). However, the main difference is that in a defocusing medium the potential has a local minimum, thus the propagation is expected to be stable.

Next, we consider the case when the laser beam is focused with a positive lens (creating an initial converging beam wave front). This might change significantly the characteristics of the beam propagation, depending on the initial beam radius and the focal length of the converging lens. We consider the case of a beam being focused by a positive lens with a focal length $f=150$ cm (we choose this particular value in order to make a comparison with experimental results). First, we consider a larger beam radius $a_0=0.55$ cm. In Fig. 3(a) the potential is plotted without the lens (collimated beam) (solid line) and using the lens (converging beam) (dotted line). As it can be seen for a collimated beam the potential crosses at two points on the axis which would

result in an oscillatory solution discussed earlier. However, in the presence of a converging lens, the effect of the lens has pushed down the potential such that it only crosses at one point of the axis which is the point where self focusing is stopped. In this case the solution corresponds to the case in which the particle is pushed at $a=1$ (in other words the lens provides an initial kinetic energy to the particle), and the particle as before will come to rest at some $a_{\min}$, however, on the way back, since the potential does not cross the axis it will escape to infinity, causing diffraction. The solution to this case is given in Fig. 3(b), in agreement with our qualitative discussion. As the initial power is further increased the initial gap created by the lens effect will close, in other words the potential will eventually cross two points on the axis. However, this may occur at very high input powers. As the initial beam radius is decreased the effect of the lens becomes negligible. In our analysis, there is a transition around $a_0=0.1$ where the lens effect becomes less important. Thus the beam radius as well as the focal length of the lens (i.e., curvature of the beam front) have an important effect on the beam propagation, which will become more apparent in the next section. It is important to note that the period as well as the amplitude of these oscillations depend strongly on the input power and beam radius. For a larger beam radius the refocusing occurs at further distances than with a smaller beam diameter. In addition, for a given initial beam radius the distance between focusing and refocusing decreases as the initial power is increased.

2. Dynamics of the entire pulse

To make a connection with specific experiments we consider that the laser beam is focused with a lens of focal point $f=150$ cm. We start by setting $g(\tau)=1$, which would correspond to a case where defocusing is created by a higher-order nonlinear susceptibility. First, we consider an input beam radius $a_0=0.55$ cm and initial power $P_0=5.0$. In Fig. 4, we plot the on-axis peak intensity as a function of the propagation distance (we define the on-axis intensity as the global maximum value of the pulse for the transverse coordinate $r=0$) (solid line). It can be seen that the beam focuses before the linear focal point due to self focusing but then diffracts after the geometrical focal point. The dotted and dotted-dashed lines correspond to two different pulse slices for $\tau=0$ and $\tau=-0.5$ (in units of $\tau_0=187$ fs), respectively, which correspond to slices that are above the critical power for self focusing. The long-dash line on the other hand corresponds to a time slice ($\tau=-1.25$) that is below the critical power so that self focusing does not take place, and the maximum of the intensity occurs between $z_L=f/[1+(f/z_R)^2]$ and f.

In Fig. 5 we plot the on-axis temporal intensity profile for $z=145$ cm (solid line) and $z=147$ cm (dotted line). As can be seen the pulse is reshaped around the focal region, in which two peaks appear, that on further propagation separate from each other. The peak of the leading pulse is shifted towards earlier times. This is consistent with previous numerical simulations [3,5,6]. However, the appearance of the second peak behind the leading one would be suppressed since it interacts with the plasma. In addition, this reshaping can significantly differ when the retarded Kerr nonlinearity and/or group velocity dispersion (GVD) are taken into account [5,6]. The important result is that as the pulse approaches the focal region a strong reshaping of the pulse occurs. This is a consequence of the combined effect of self focusing and defocusing. The strongest slice ($\tau=0$) focuses first. Other slices will focus further away. Around the focal point the $\tau=0$ slice has started to defocus, but the earlier slices are still coming to a focus. Thus when looking at that propagation distance we see the reshaping of the pulse. The fact that each time slice experiences a different portion of the defocusing can be qualitatively accounted for by considering $g(\tau)=0.5(2+\tau)$. In Fig. 6, the on-axis intensity is plotted for the same initial conditions as in Fig. 4. Here, some of the early slices ($\tau<0$) experience less defocusing and reach a higher intensity in order to stop the focusing. As a result the

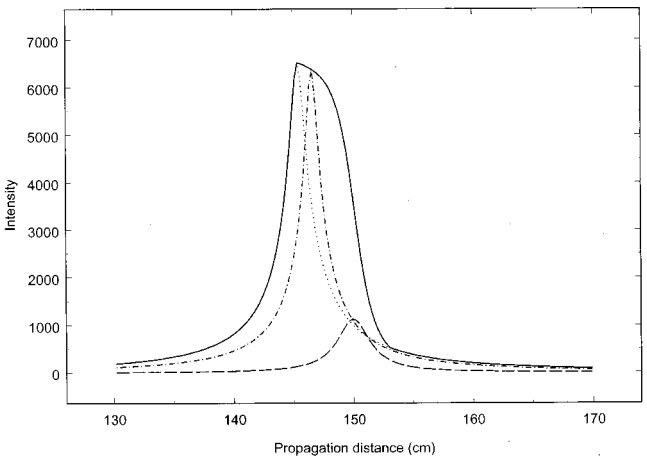

FIG. 4. Plotted is the on-axis intensity (in units of P_{cr}/a_0^2) (solid line) for the case of a pulsed laser beam focused by a converging lens with $f=150$ cm, $P_0=5$, $a_0=0.55$ cm, and $g(\tau)=1.0$. The behavior of different slices of the pulse are plotted for $\tau=0$ (dotted line), $\tau=-0.4$ (dash-dotted line) and $\tau=-1.0$ (dash line). Slices that are above the crtical power for selffocusing focus before the geometrical focal point whereas slices that are below crtical power (dash line) come to a focus between the linear focal point z_L and the geometrical focal point.

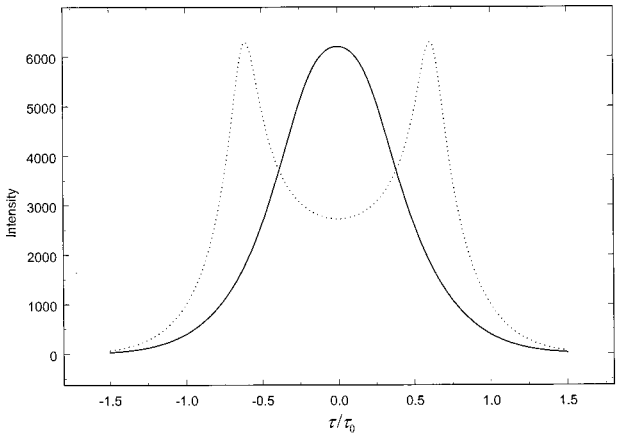

FIG. 5. The on-axis temporal intensity profile in the retarded time coordinate τ/τ_0 are plotted for $z=145$ cm (solid line) and $z=147$ cm (dotted line). The intial conditions are the same as in Fig. 4. Around the focal point two peaks appear, which get separated temporally away from each other on further propagation.

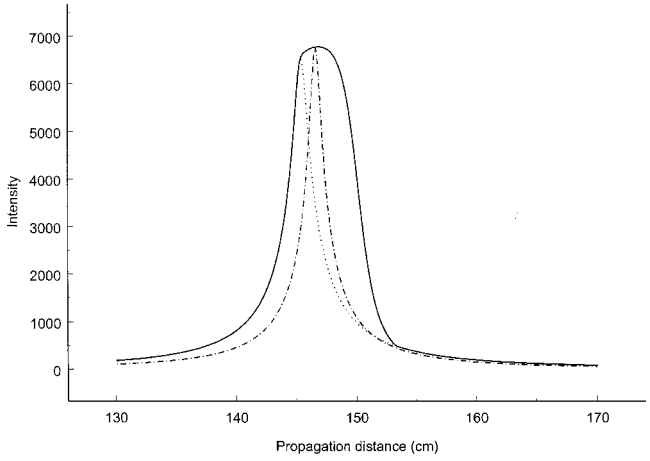

FIG. 6. Plotted is the on-axis intensity for the same condition as in Fig. 4 except that here $g(\tau)=0.5(2+\tau)$. Due to the fact that earlier slices of the pulse (dotted-dash line) see a smaller defocusing and consequently reach a higher intensity in order to stop the self focusing. This in turn creates a more smoother on-axis intensity profile when compared with Fig. 4. The result is in qualitative agreement with the experimental observation given in Fig. 7(a).

overall on-axis intensity profile is smoother when compared to Fig. 4.

In previous experiments the critical power for self focusing in air was estimated to be in the range of 6-10 GW [1,3]. In the present mentioned experiment this would correspond to about $1.5-2.5$ mJ. In the experiment performed by the group at Laval University, the photon signal of both N_2 and N_2^+ are collected along the propagation direction for various input energies. The photon signal is related to the peak intensity of the pulse, the higher the intensity, the higher is the photon signal [7]. In Fig. 7(a) the experimental results are shown for an input beam radius of 0.55 cm. Up to 20 mJ the intensity profile is approximately symmetric with respect to the maximum intensity and only one focal point is present. This is in good agreement with our variational result, where no refocusing occurs beyond the geometrical focal point as seen in Fig. 6.

As the initial pulse energy is increased further the on-axis intensity does not fall rapidly beyond the geometrical focal point in which a shoulder is developed [see Fig. 7(a)]. One possible explanation to this phenomenon might be due to absorption losses. In Fig. 8, the on axis intensity is plotted for $a_0=0.55$ cm in the presence of multiphoton absorption. As we can see there is a shoulder beyond the geometrical focal point in the presence of losses (solid line) when compared without any losses (dotted line). One can explain this effect in terms of the mechanical analogy in which the particle loses sufficient energy to be trapped in the well for a while causing small oscillations.

When the initial beam radius is increased even further the potential is pushed further down by the lens effect such that one would expect the on-axis intensity to resemble the one given in Fig. 6. In fact this has been seen experimentally at Laval University where they used a beam with radius of 1 cm focused by a lens with $f=100$ cm, and a pulse energy of 20 mJ. The one axis intensity shows a behavior similar to the one shown in Fig. 6. The effect of the focal length on the pulse propagation was also observed experimentally by

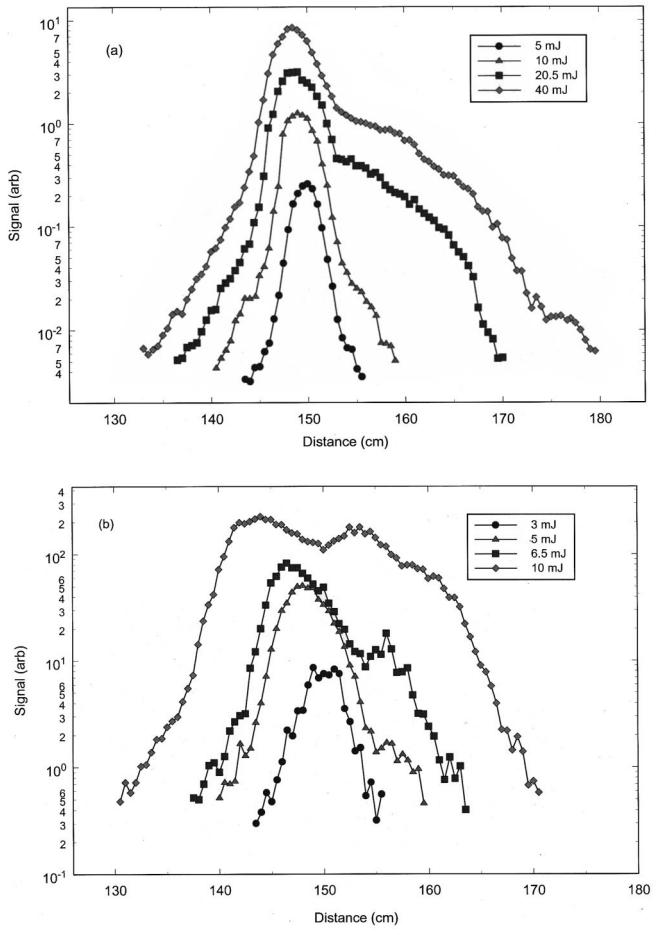

FIG. 7. Shown are the experimental results obtained by the group at Laval University (Ref. [7]). The experimental setup corresponds to the case of a 220-fs laser pulse focused by a converging lens with $f=150$ cm for an initial beam radius of (a) 0.55 cm and (b) 0.2 cm, for various input energies. The signal corresponds to the photon signal from both N_2 and N_2^+ which is related to the peak intensity of the pulse. The higher the intensity, the higher is the photon signal.

Nishioka *et al.* [18]. They observe no filament formation when a smaller focal length was used, which is consistent with our analysis.

On the other hand, when the beam radius is reduced to 0.05 cm a dramatic change occurs in the propagation. From the previous analysis we showed that the beam undergoes an oscillatory behavior. In Fig. 9, we plot the on-axis intensity as a function of z for $g(\tau)=1$. The situation is now significantly different than the previous case where there was no refocusing. As can be seen from Fig. 9 each slice above the critical power refocuses again, but at different locations. When we look at the overall on-axis intensity we see that the pulse first focuses and then defocuses and focuses again and this may repeat itself at further distances but it is not as apparent as the first one. The refocusing of the pulse has been previously observed in numerical simulations [3,5,6]. It seems that as the pulse further propagates the on-axis intensity appears to be unchanged despite the fact that all the different slices still oscillate. However, it is important to note that although the intensity remains unchanged over a long distance this is quite different than the usual self guiding

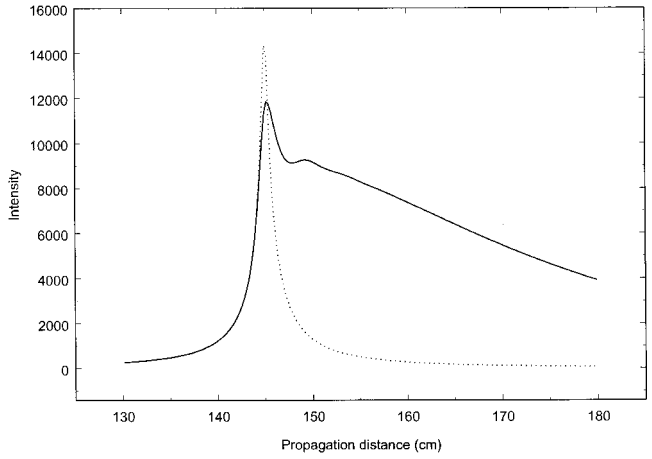

FIG. 8. The effect of multiphoton absorption is shown for the propagation of a laser beam with $a_0=0.55$ cm focused by a lens with $f=150$ cm. In the presence of multiphoton absorption losses (solid line) the beam significantly propagates beyond the geometrical focal point when compared for the case without absorption losses (dotted line).

mode discussed first by Chiao *et al.* [19]. Here, the situation is more dynamic and involves both the temporal as well as spatial variation of the laser beam.

Perhaps, a more interesting aspect of the pulse propagation is the reshaping of the pulse during propagation. As we have shown in the previous case, there is a significant reshaping of the pulse whenever the pulse starts to focus. This phenomenon also occurs in this case but it is more dynamic. In Fig. 10, the temporal on-axis intensity profile is plotted as a function of the propagation distance. In Fig. 9, we see that around $z=40$ cm the pulse has come to a focus, when compared with Fig. 10 we see the reshaping of the pulse around

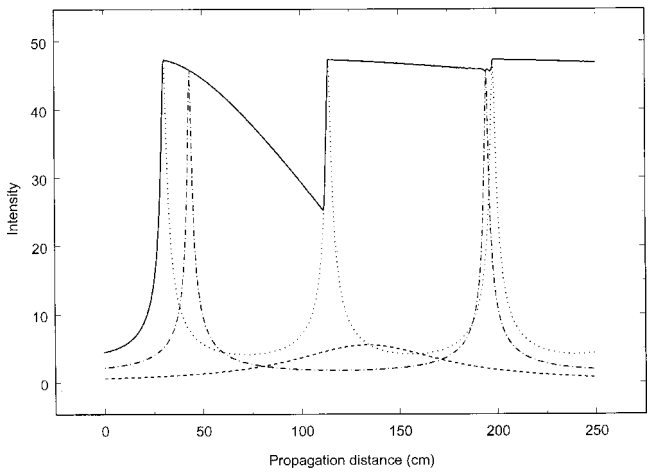

FIG. 9. Plotted is the on-axis intensity (solid line) for $a_0=0.05$ cm, $P_0=7$, and $g(\tau)=1.0$. The propgation properties have significantly changed when comparing with the case of $a_0=0.55$ cm shown in Fig. 4. Different slices of the pulse are plotted as a function of propagation distance. For slices that are above the critical power (dotted line) and (dash-dotted line), show an oscillatory behavior, whereas for a slice below critical power (dash line) the slice exhibits only one focal point. The superposition of all these different time slices creates an overall on-axis intensity profile shown by the solid line.

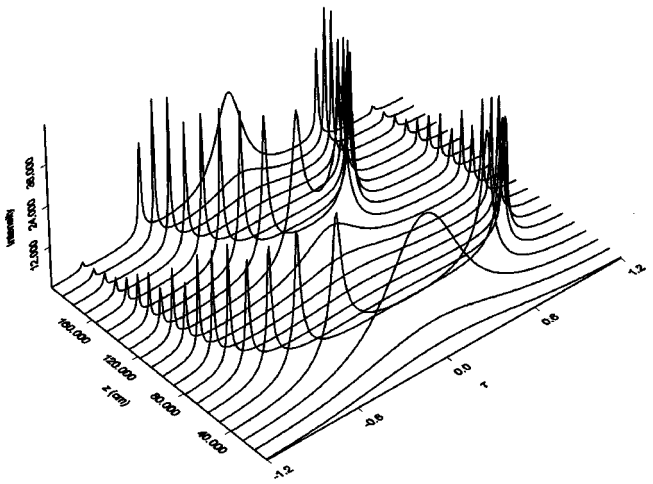

FIG. 10. Plotted is the on-axis temporal intensity profile in the retarded time coortinate τ (in units of τ_0) for the same initial conditions as in Fig. 9. When compared with Fig. 9, it can be seen whenever the pulse refocuses it undergoes a pulse reshaping process in which two peaks start to develop. This is clearly seen around $z=40$ cm and $z=120$ cm.

that point. Again from Fig. 9 it can be seen that a second refocusing occurs around $z=120$ cm, which manifests itself as a second pulse reshaping process as it can be seen in Fig. 10. This observation agrees qualitatively with previous numerical simulations [3,5,6]. In Ref. [6], the pulse splitting is clearly demonstrated in their numerical simulations for an instantaneous Kerr response. The two pulses then separate further away from each other upon further propagation, which is also seen in our calculations. The subsequent reshaping of the pulse and a secondary splitting has also been shown in Ref. [5]. The main difference between their result and ours is in the quantitative temporal shape of the pulse. The physical reason for the reshaping of the pulse comes from the fact that each slice focuses and refocus at different positions, so that at a given position one slice might come to a minimum whereas another slice might be at its maximum. Consequently, when we look at a certain position we see the pulse being reshaped. This reshaping process will further be affected when other effects such as GVD and/or retarded Kerr nonlinearity are included in the propagation model [5,6]. However, in our model we can identify explicitly the reshaping of the pulse when it refocuses again.

In Fig. 11, we plot the on-axis intensity for two different input powers. It can be seen that for higher input powers the dip in the on-axis intensity becomes smaller; this feature is consisted with experimental result [7] [see Fig. 7(b)]. In addition we see that the minimum point for the on-axis intensity further away from the lens for higher input powers, in agreement with the experimental observation [7]. It is also important to emphasize that this refocusing phenomenon does not appear very strongly in the case of a 0.275 cm laser beam. The experimental results have not been analyzed completely, but it is clear that there is a significant difference in the propagation between a 0.275 and 0.2 cm beam radius. Such a transition is clearly seen in our analysis as well. In our analysis the transition appears around a beam radius of 0.1 cm, which is much lower than the experimental observation. However, this discrepancy can be attributed to our ap-

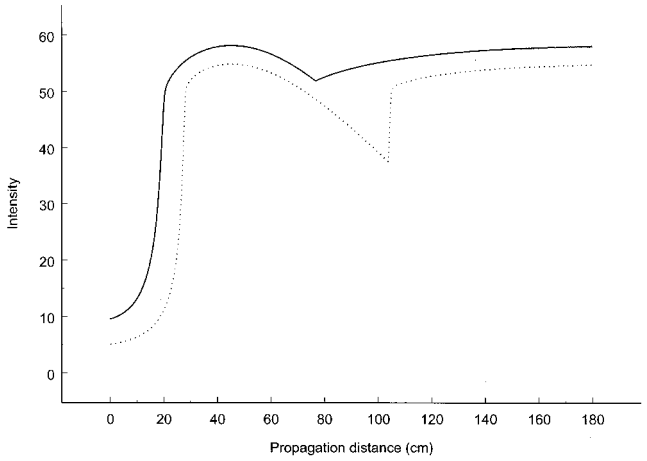

FIG. 11. On-axis intensites for $a_0=0.05$ cm with $P_0=15$ (solid line) and $P_0=8$ (dotted line). For higher input powers the minimum point for the on-axis intensity moves away from the lens, and the minimum dip becomes smaller. This is in agreement with the experimental observation shown in Fig. 7(b). Here $g(\tau)=0.5(1.55+\tau)$.

proximate method. In summary, we can explain the origin of the refocusing phenomenon from a simple model which is in qualitative agreement with the experiment [7].

D. Effect of higher-order nonresonant susceptibility ($\beta\neq 0, \gamma\neq 0$)

In the previous section, we have shown how the plasma generation through multiphoton ionization can lead to a balance between self focusing and defocusing. It is clear from Eqs. (17)–(19) that if there are any other higher-order contributions to the nonlinear susceptibility function, they may have an important role in the defocusing process. Here, we show that if there is a negative $\chi^{(5)}$ effect it can significantly contribute to the defocusing process depending on the magnitude of the $\chi^{(5)}$ value. Let us assume that $\chi^{(5)}=-3.6\times10^{-29}$(esu) which corresponds to $n_4=10^{-32}$ cm^4/W^2. To demonstrate the effect of $\chi^{(5)}$ we consider only one particular slice of the pulse namely $\tau=0$ and a collimated beam with a beam radius $a_0=0.5$ cm. In Fig. 12, the peak intensity (normalized to the input intensity I_0) is plotted as a function of z (in units of ka_0^2). The solid and dotted lines represent the case when the defocusing is entirely due to multiphoton ionization and $\chi^{(5)}$, respectively. The dotted-dashed line includes the effect of both multiphoton ionization and $\chi^{(5)}$. It can be seen in Fig. 12(a) that when the input power is just above the critical power the $\chi^{(5)}$ effect dominates the defocusing process, and depending on the conditions a strong plasma may not be generated in this regime. On the other hand, when the input power is well above the critical power, then both the ionization and $\chi^{(5)}$ contribute to the defocusing process [see Fig. 12(b)]. In this case both effects may not be separated from each other, and clearly a strong plasma would be generated as well. Furthermore, if the sign of $\chi^{(5)}$ is positive then we may have a case where even more plasma is generated in order to overcome additional focusing due to a positive $\chi^{(5)}$. As we pointed out

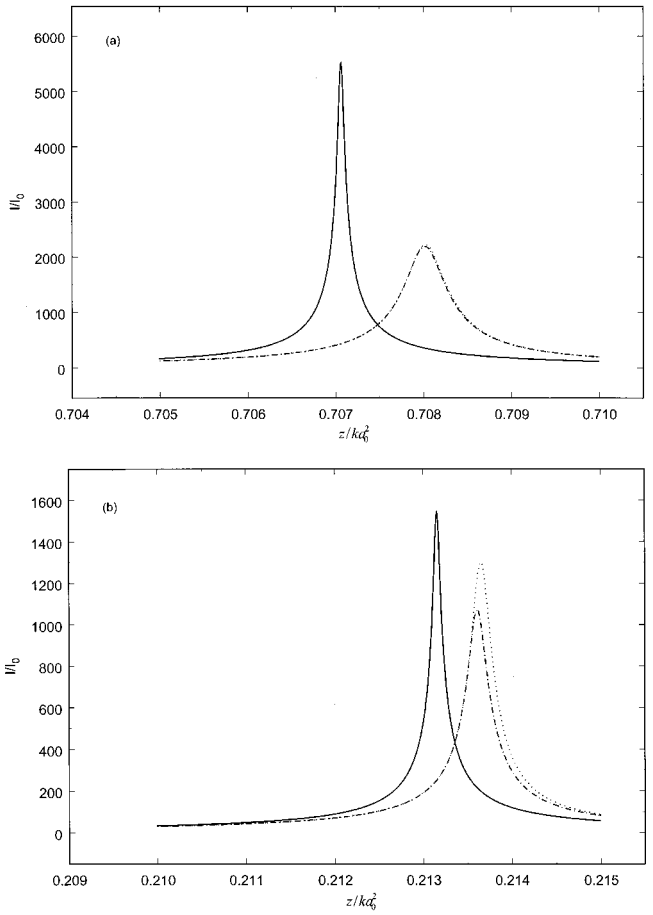

FIG. 12. Plotted are the normalized peak intensities as a function of z (in units of ka_0^2) and $\tau=0$, for (a) $P_0=1.5$ and (b) $P_0=6.5$. The solid line and dotted line represent when the defocusing is entirely due to the multiphoton ionization and $\chi^{(5)}$, respectively. Whereas the dotted-dash line includes both ionization and $\chi^{(5)}$ contributions. It can be seen when the input power is just above the critical power the $\chi^{(5)}$ is dominant, whereas well above the critical power both ionization and $\chi^{(5)}$ and contributions are important. Here $\chi^{(5)}=-3.6\times10^{-29}$(esu).

earlier, at this point we do not have specific values on the magnitude and sign of the $\chi^{(5)}$ coefficient for nitrogen or oxygen. Thus whether higher-order susceptibility terms have an effect will rely on further experimental studies.

III. CONCLUSION

In conclusion, we have demonstrated that using an analytical method many of the properties of the femtosecond pulse propagation in air can be explained in a much simpler physical form than previously studied. The most important result is the fact that we are able to show that the defocusing created by the plasma generation can be described, at least qualitatively, as an effective higher-order $\chi^{(n)}$ like effect. This connection provides a much more transparent interpretation of the pulse propagation phenomenon in air. Furthermore, certain connections can be made between the pulse propagation in an ionizing medium and in a saturable or $\chi^{(5)}$ medium. Using our method, we were not only able to recapture some of the previous numerical simulations and provide

analytical interpretation, but we obtained qualitative agreement with experimental results as well. In this respect our approach could be used to make certain predictions and can guide the numerical simulations.

The possible effect of higher-order nonresonant susceptibilities, namely a $\chi^{(5)}$ effect is described qualitatively. We showed that although the magnitude of $\chi^{(5)}$ is small it can contribute significantly to the defocusing process. Since we do not have specific values for the sign or the magnitude of $\chi^{(5)}$ we are not able to provide absolute conclusions.

ACKNOWLEDGMENTS

We would like to acknowledge Dr. M. Scalora for critically reading this manuscript and for his valuable suggestions on various portions on this work. One of us (N.A.) acknowledges the financial support of the National Research Council.

[1] A. Braun, G. Korn, X. Liu, D. Du, J. Squier, and G. Mourou, Opt. Lett. **20**, 73 (1995).

[2] E.T.J. Nibbering, P.F. Curley, G. Grillon, B.S. Prade, M.A. Franco, F. Salin, and A. Mysyrowicz, Opt. Lett. **21**, 62 (1996); P.F. Curley, E.T.J. Nibbering, G. Grillon, R. Lange, M.A. Franco, T. Lehner, B. Prade, and A. Mysyrowicz, in *Ultrafast Phenomenon X*, edited by P. F. Barbara, J. G. Fujimato, W. H. Knox, and W. Zinth (Springer-Verlag, Berlin, 1996), Vol. 62, p. 103; H.R. Lange, G. Grillon, J.F. Ripoche, M.A. Franco, B. Lamouroux, B.S. Prade, and A. Mysyrowicz, Opt. Lett. **23**, 120 (1998); S. Tzortzakis, M.A. Franco, Y.-B. André, A. Chiron, B. Lamouroux, B.S. Prade, and A. Mysyrowicz, Phys. Rev. E **60**, R3505 (1999).

[3] A. Brodeur, C.Y. Chien, F.A. Ilkov, O.G. Koserava, and V.P. Kandidov, Opt. Lett. **22**, 304 (1997); O.G. Kosereva, V.P. Kandidov, A. Brodeur, C.Y. Chien, and S.L. Chin, *ibid.* **22**, 1332 (1997); O.G. Kosereva, V.P. Kandidov, A. Brodeur, and S.L. Chin, J. Nonlinear Opt. Phys. Mater. **6**, 485 (1997); S.L. Chin, A. Brodeur, S. Petit, O.G. Koserava, and V.P. Kandidov, *ibid.* **8**, 121 (1999).

[4] L. Wöste, C. Wedekind, H. Wille, P. Rairoux, B. Stein, S. Nikolov, C. Werner, S. Niedermeier, F. Ronneberger, H. Schillinger, and R. Sauerbrey, Laser Optoelektron. **29**, 51 (1997); H. Schillinger and R. Sauerbrey, Appl. Phys. B: Lasers Opt. **68**, 753 (1999).

[5] M. Mlejnek, E.M. Wright, and J.V. Moloney, Opt. Lett. **23**, 382 (1998); Optics and Photonics News, December, 37 (1998); M. Mlejnek, M. Kolesik, J.V. Moleney, and E.M. Wright, Phys. Rev. Lett. **83**, 2938 (1999).

[6] A. Chiron, B. Lamouroux, R. Lange, J.-F. Ripoche, M. Franco, B. Prade, G. Bonnaud, G. Riazuelo, and A. Mysyrowicz, Eur. Phys. J. D **6**, 383 (1999).

[7] A. Talebpour, S. Petit, and S.L. Chin, Opt. Commun. **171**, 285 (1999).

[8] X.M. Zhao, J.-C. Diels, C.V. Wang, J.M. Elizondo, IEEE J. Quantum Electron. **31**, 599 (1995); X. M. Zhao, S. Diddams, and J.-C. Diels, in *Tunable Laser Applications*, edited by F. J. Duarte (Marcel Dekker, New York, 1995), p.113.

[9] D. Anderson and M. Bonnedal, Phys. Fluids **22**, 105 (1979); D. Anderson, Phys. Rev. A **27**, 3135 (1983); M. Deaix, D. Anderson, and M. Lisak, J. Opt. Soc. Am. B **8**, 2082 (1991).

[10] S.C. Cerda, S.B. Cavalcanti, and J.M. Hickmann, Eur. Phys. J. D **1**, 313 (1998).

[11] A. Talebpour, J. Yang, and S.L. Chin, Opt. Commun. **163**, 29 (1999). There are two printing errors in this paper. In Eq. (2) Z should read Z_{eff}, and in Eq. (8) W_m should be w_m. The $\times$ sign should not be there.

[12] J.D. Jackson, *Classical Electrodynamics* (McGraw-Hill, New York 1975).

[13] E.T.J. Nibbering, G. Grillion, M.A. Franco, B.S. Prade, and A. Mysyrowicz, J. Opt. Soc. Am. B **14**, 650 (1997).

[14] Y.R. Shen, *The Principles of Nonlinear Optics* (Wiley, New York, 1984).

[15] N.L. Manakov and V.D. Ovsyannikov, Zh. Éksp. Teor. Fiz. **79**, 1769 (1980) [Sov. Phys. JETP **52**, 895 (1980)].

[16] A. L'Huillier, L. Lompré, G. Mainfray, and C. Manus, in *Atoms in Intense Laser Fields*, edited by M. Gavrila (Academic Press, 1992), pp.139–201.

[17] J.H. Marburger and W.G. Wagner, IEEE J. Quantum Electron. **3**, 415 (1967); G.L. McAllister, J.H. Marburger, and L.G. DeShazer, Phys. Rev. Lett. **21**, 1648 (1968).

[18] H. Nishioka, W. Odajima, K-I. Ueda, and H. Takuma, Opt. Lett. **20**, 2505 (1995).

[19] R.Y. Chiao, E. Garmire, and C.H. Townes, Phys. Rev. Lett. **13**, 474 (1964).